Building new entities from existing titanium part by electron beam melting: microstructures and mechanical properties

Guillaume Mandil, van Thao Le, Henri Paris, Mathieu Suard

Noname manuscript No.
(will be inserted by the editor)

Building new entities from existing titanium part by Electron Beam Melting: Microstructures and mechanical properties

Guillaume Mandil · Van Thao Le · Henri Paris · Mathieu Suard

Received: date / Accepted: date

Abstract Electron Beam Melting (EBM) has been recognized as an emerging additive manufacturing technology, which allows the production of fully dense parts from various metals. The technique builds parts using an electron beam to melt metal powder, layer by layer, in a powder bed. Thus, complex parts, including internal structures, can be made directly from 3D CAD models without special fixtures and cutting tools. Much research is conducted to study the microstructure and mechanical properties of EBM-built parts, or to investigate the effects of EBM process parameters on the quality of parts. However, using EBM for building new features on an existing part has received little attention from the research community. Due to its performance, EBM seems able to transform an End-of-Life (EoL) part/existing part into a new part without returning to the level of raw material. The aim of this study is to validate such principle. In this paper, an EBM machine was used to produce new Ti-6Al-4V features on a Ti-6Al-4V plate, which was considered as a useful core retrieved from an EoL product. The built samples, including EBM-built features and Ti-6Al-4V plate, were investigated in terms of their microstructure and mechanical properties. The results showed that EBM technique allows new features with a suitable microstructure and controlled mechanical properties to be built on an existing part. Moreover, the EBM-built features have a strong bond with the existing part leading to the same mechanical characteristics as original part. These demonstrate that the EBM technology has a promising potential for producing new parts from EoL parts/existing parts.

Keywords Additive manufacturing · Electron beam melting · Ti-6Al-4V · Microstructure · Mechanical properties

G. Mandil[1,*] · V.T. Le[1,2] · H. Paris[1] · M. Suard[1,3]
1. G-SCOP Laboratory, Grenoble-Alpes University, 46, avenue Félix Viallet, 38031 Grenoble Cedex 1, France.
2. Le Quy Don Technical University, 236 Hoang Quoc Viet Str., Cau Giay Dist., Hanoi City, Vietnam.
3. SIMaP Laboratory, Grenoble-Alpes University, 1130, rue de la piscine, 38402 Saint Martin d'Hères, France.
∗ Corresponding author. Tel.: +33476574776 E-mail: Guillaume.Mandil@g-scop.eu

1 Introduction

Nowadays, additive manufacturing (AM) has emerged as a promising fabrication technology for metal parts. Since the late 1980s, AM technologies have been investigated and some were made commercially available, such as selective laser melting (SLM), laser metal deposition (LMD) and electron beam melting (EBM) (as presented in previous publications [1, 2, 3, 4]). In comparison to conventional manufacturing processes, AM technologies make it possible to produce parts directly from 3D CAD models by adding materials layer by layer [5]. They offer the beneficial ability to build complex parts without special fixtures and cutting tools [1, 3]. AM processes can produce end-use parts in a significantly short time, and they are cost-effective for single parts and small to medium batches [1, 6]. Furthermore, due to the ability of AM technologies, the topologically optimized design can increase the functionality of products; and, lightweight parts can be realized [7, 8]. Hence, an amount of energy and auxiliary resources required, as well as CO_2 emissions during manufacturing process can be reduced [9, 10, 11]. Moreover, AM techniques are interesting in the sense that they reduce scrap generation compared to conventional manufacturing techniques [10]. Today, AM has a wide application in auto-

motive, aerospace industry and biomedical engineering [1]. It is very likely that AM will have a significant societal impact in the near future.

More particularly, the EBM technology developed by Arcam in Sweden is today considered as a revolutionary AM technology. EBM has emerged as a potentially cost-effective process for high-value, small-batch productions for biomedical and aerospace applications [12]. This process offers a high build rate due to the unique characteristics of an electron beam, such as high energy density, high adsorption rate, and high scan speed [9, 13, 14]. In addition, the entire EBM process takes place under secondary vacuum that provides a clean atmosphere to prevent the contamination of metal parts during the building process; thus, parts with excellent properties can be achieved [9, 14].

In recent years, EBM has been successfully used in AM with various metals. For example, Murr et al. [15] produced titanium aluminide alloy components via EBM. Cormier et al. [16] fabricated parts made of tool steel. Murr et al. [17, 18] manufactured EBM parts made of nickel-base superalloy. Ramirez et al. [19] and Frigola et al. [20] also fabricated copper components by EBM. These studies have demonstrated that EBM is capable of building fully dense metal parts with excellent properties. However, Koike et al. [21] and Suard et al. [22] showed that EBM produced surface presents a significant roughness, containing a rippled structure with visible sintered powder grains. Thus, the as-produced surface roughness achieving by EBM may be unfavorable, especially for products where a smooth surface is required. Among the materials, titanium alloys (e.g., Ti-6Al-4V) have been largely used in EBM, as well as in metal additive manufacturing research. In fact, titanium alloys are extensively used in aerospace industry and in biomedical applications because of their high mechanical strength, lightweight, corrosion resistance, and good biocompatibility [9, 23]. However, they are often difficult to cut due to a relatively low thermal conductivity, and also difficult to cast because of its high reactivity with oxygen or the mold [24]. In addition, the use of traditional techniques makes it difficult to manufacture highly complex and functional titanium alloy parts [9, 24].

Much research has been conducted to study the microstructure and mechanical properties of Ti-6Al-4V parts produced by EBM process. Koike et al. [21] investigated mechanical properties, and grindability, and corrosion resistance of Ti-6Al-4V ELI (Extra Low Interstitials) EBM-built specimens. They found that EBM-built specimens have an α/β lamellar microstructures with a rough surface. Their ultimate tensile strength (UTS) and the yield stress (YS) were comparable to those of cast and wrought specimens. Koike et al. [25] and Rafi et al. [26] also compared SLM and EBM processes in terms of microstructures, mechanical properties of Ti-6Al-4V ELI specimens. In these studies, the strength of EBM-built specimens was slightly lower than that of SLM- and wrought- built specimens. However, Facchini et al. [27] found that the UTS and YS of Ti-6Al-4V EBM-built specimens were higher than those of wrought and annealed material. Murr et al. [28] and Rafi et al. [26] demonstrated that the elongation of EBM-built specimens was higher than that of SLM-built specimens, but the hardness of SLM-built specimens was higher than that of EBM-built specimens. These were due to the harder martensitic phase of SLM-built specimens when compared to the softer α phase of EBM-built specimens [26]. Due to the finer α/β lamellar microstructures, the hardness of EBM-built specimens was higher than that of wrought specimens [21, 25]. Table 1 summarizes mechanical properties of Ti-6Al-4V EBM-built specimens versus Ti-6Al-4V SLM- and wrought- built specimens.

Other researchers have investigated the effects of process parameters and scanning strategy on the microstructure, mechanical properties and the surface roughness of EBM-built parts. Syam et al. [30] investigated the effects of scanning velocity, beam current, beam defocusing current and energy density on the surface roughness of EBM-built thin wall components. Karlsson et al. [24] used two different size powders and two build layer thicknesses to produce components in EBM process. They concluded that the material properties were not significantly affected by powder size or layer thickness. Recently, Guo et al. [31] also investigated the effects of scanning parameters, such as beam current, scanning velocity, etc., on surface appearance and microstructures of Ti-6Al-4V EBM-built parts. They found that the scanning parameters and the scanning frequency have a significant influence on the material deposition. The samples built by using various scanning parameters can be classified into three types: (I) porous surface with internal cavities; (II) dense and flat surface with pores at edge; and (III) wavy surface. In the samples of type II and III, the microstructures were dominantly α/β phase. Weiwei et al. [32] presented that the preheating step, namely preheating the substrate before depositing and preheating the powder layer before melting the cross-section, could slightly sinter the powder bed. This reduces the risk of powder blow away (by increasing the thermal and mechanical conductiv-

Table 1 Mechanical properties of AM-built specimens and wrought-produced specimens

Process	Material	YS (0.2 %) (MPa)	UTS (MPa)	Elongation (%)	Hardness (HV)	Ref.
EBM	Ti-6Al-4V	910 - 940	950 - 990	14 - 16	300 - 345	Arcam [1]
	Ti-6Al-4V ELI	735	775	2.3	369	[21]
	Ti-6Al-4V ELI	869	928	9.9	327	[26]
	Ti-6Al-4V	830 ± 5	915 ± 10	-	327	[27]
	Ti-6Al-4V	1100 - 1150	1150 - 1200	16 - 25	427	[28]
	Ti-6Al-4V	884 - 939	994 - 1031	12 - 14	-	[29]
SLM	Ti-6Al-4V ELI	1143	1219	4.89	400	[26]
	Ti-6Al-4V	1350 - 1400	1450 - 1500	4 - 5	507	[28]
Wrought	Ti-6Al-4V ELI	860	931	14	327	[21]
	Ti-6Al-4V	790 ± 20	870 ± 10	-	-	[27]

ity), and also maintains the powder bed at a high build temperature. More importantly, preheating can reduce residual stress by bringing down the temperature gradient between successive layers during processing [26]. Al-Bermani et al. [29] also stated that the build temperature has a significant effect on the properties and microstructure of built parts. In the case of Ti-6Al-4V built parts, each layer was often heated to 750^{o}C for pre-sintering the powder bed [13, 22].

Much research has been focused on understanding the EBM process and the resulting properties of fabricated parts. However, limited research has been focused on exploring the feasibility of using EBM technology for remanufacturing or repair of high-value parts. Other AM technologies used for remanufacturing or repairing high-value parts have been published in the literature. For example, laser metal deposition (LMD) technology was used to successfully repair (or remanufacture) valuable tools and dies [33, 34]. Wilson et al. [35] showed that laser direct deposition was efficient for the remanufacturing of turbine blades and that its ability adapts a wide range of part defects. Nan et al. [36] presented a three-dimensional laser remanufacturing system (LRS) based on the integration of reverse engineering and laser cladding. This method was able to extend the life-time of aging dies, aircrafts, vehicle components. They have also shown the advantages of such system, such as reducing the lead-time, keeping the heat affected zone to minimum, and low cost of maintaining critical parts. In other research, Cottam et al. [39] investigated laser cladding of Ti-6Al-4V powder on Ti-6Al-4V substrate to determine laser parameters that could be used for repairing Ti-6Al-4V parts. Their experimental method seems similar to our work. However, they focused their investigation on the effect of different process parameters on the microstructure and microhardness of built parts. In their work, Dutta et al. [37] mentioned that directed energy deposition processes - e.g., direct metal deposition (DMD), or construction laser additive (CLAD) - have a potential application for remanufacturing and repairing parts, as well as for adding new features to existing parts because of the large and flexible build envelope of a 5-axis machine. On the other hand, remanufacturing using powder bed processes (e.g., SLM, EBM) has to start from a flat surface. It represents a significant limitation [37]. However, these processes can be adequate for a wide range of small and medium and complex parts. Recently, Terrazas et al. [38] presented a method, which allows the fabrication of multi-material metallic components using discrete runs of EBM system. In this work, the authors successfully built a copper entity on the top of an existing titanium part. In particular, they studied the influence of the build direction and the obtained microstructures and hardness. Their results open the perspective of using EBM for remanufacturing.

The aim of this study is to validate the feasibility of EBM technique to produce a new entities from an EoL part/existing part. In current work, an A1 EBM machine from Arcam® was used to build new Ti-6Al-4V features on Ti-6Al-4V plates, which were considered as existing parts. Then, the built samples were investigated in term of their microstructure and mechanical properties. This allowed us to verify a strength of the mechanical bonding between the EBM-built features and the titanium plate.

This paper is organized into three major sections: Section 1 presents the context and the aim of this work, as well as prior studies published in the literature. Section 2 describes the materials and experimental methods. The results and discussion are presented in Section 3. Section 4 offers some conclusions and future work.

2 Materials and Methods

2.1 Materials

In this study, a standard gas atomized Ti-6Al-4V powder supplied by Arcam was used. The chemical composition of Ti-6Al-4V powder corresponds to the specification ASTM F 1472 for Ti-6Al-4V alloy wrought [14] (Table 2). The powder size distributes in the range from 40 to 120 μm with an average particle size of 70 μm. In addition, two Ti-6Al-4V rolled plates with dimensions of 150 x 150 x 25 mm were used as existing parts, on which new features were built. A built sample was used for the tensile testing, and other one was used for observation of microstructures and the hardness testing.

2.2 Electron Beam Melting (EBM) system

An A1 EBM machine from Arcam® was used to produce the samples. The principle of the process is illustrated in Fig. 1. This system consists of the electron beam compartment and the build part compartment. The system was equipped with an electron gun with an accelerating voltage of 60 kV and a maximum beam current of 50 mA. The electron-magnetic deflection lenses allow the scan speed of electron beam to reach 8000 m/s. The maximum size of build envelop is 200 x 200 x 180 mm. In order to use a high quality electron beam, as well as to reduce oxidation and contamination of titanium parts, the build environment is kept under a high vacuum (10^{-5} mbar). The build part compartment contains two powder hoppers to supply metal powder and a rake to spread the powder during the layering process on a build table. In this study, the CAD model of parts, formatted in *.stl*, is sliced into 50 μm thick cross sections by a pre-processing software. The process is carried out layer by layer using 50 μm metal powder layers. First, the powder spread out on the build table was preheated and slightly sintered by using a defocused beam, at a scan speed of 14600 mm/s and a beam current of 38 mA with 12 repetitions. Following preheating, the melting in 2D regions derived from the CAD file was conducted through two steps, i.e. contour melting and hatch melting, using a more focused and powerful beam. In the contour melting step, the electron beam was deflected rapidly and melted the contour regions of the part. Then, the hatch melting was used to fill the inner regions of the part using a beam current of 3 - 12 mA. Subsequent layers are made by lowering the build platform equivalent to the layer thickness. The process is repeated until the part is fully built.

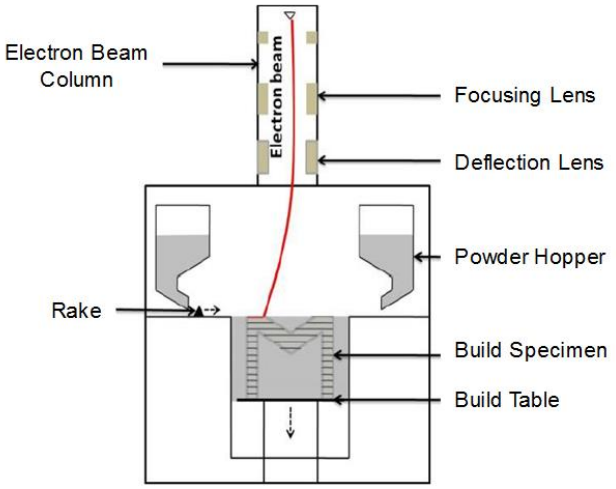

Fig. 1 Schematic drawing of an Electron Beam Melting system [22]

2.3 Fabrication of samples

For studying microstructure and microhardness, five cuboid features of 7 x 2 x 15 mm were built on the first Ti-6Al-4V plate (Fig. 2a). For the tensile testing, a specific feature with a geometry adapted with the tensile test machine was built on the second plate (as shown in Fig. 2b). The dimensions of the feature for investigating the tensile properties were 6 x 2 x 15 mm. In current study, the usual EBM process parameters (as described in Section 2.2) were used to produce these features.

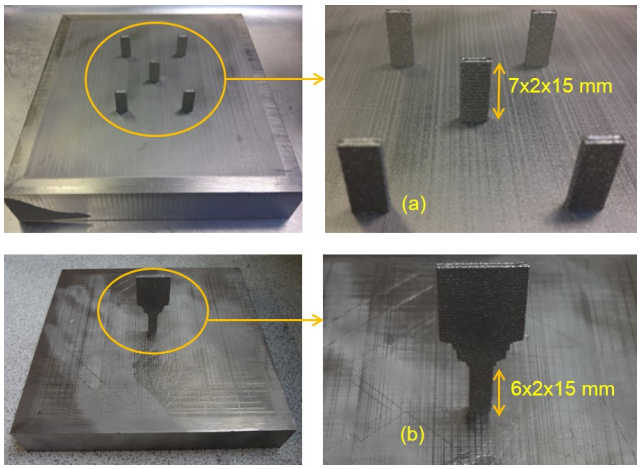

Fig. 2 Built features (a) for microstructure and the hardness testing, and (b) for the tensile testing

To build the features, a Ti-6Al-4V plate was firstly placed as a build table of EBM machine. Prior to starting the process, the electron beam scanned the plate to

Table 2 Chemical composition of the Ti-6Al-4V alloy according to ASTM F 1472

Element	Al	V	C	Fe	O	N	H	Ti
Wt%	5.5 - 6.75	3.5 - 4.5	< 0.1	< 0.3	< 0.2	< 0.05	< 0.015	Balance

heat it. The building feature process starts when the temperature at the top surface of the start plate is upper than 740^{o}C.

On the Arcam A1 machine, the thermal sensor is located under the start plate whereas the interesting temperature is the one of the top surface of the plate (see Fig. 3a). As titanium start plate has a high thickness (25mm) and thermal conductivity compared to standard 10mm thick stainless steel start plates, a rough relation between the temperatures of the top and bottom surfaces has to be determined. For that purpose, the titanium plate was heated by the electron beam until the bottom surface reaches 550^{o}C. At that point (see Fig. 3b), the heating was stopped; and, the variations of the bottom temperature was tracked. After the heating was stopped, we observed that the temperature of the bottom surface increased to reach 567^{o}C in about one minute and then decreased. In a first approximation, little heat was assumed to be dissipated in one minute, meaning that the linear gradient of temperature in the plate during heating is about 20^{o}C. Consequently, in order to obtain a temperature of the top surface of the titanium start plate at 740^{o}C, the thermal sensor has to measure around 720^{o}C under the bottom surface.

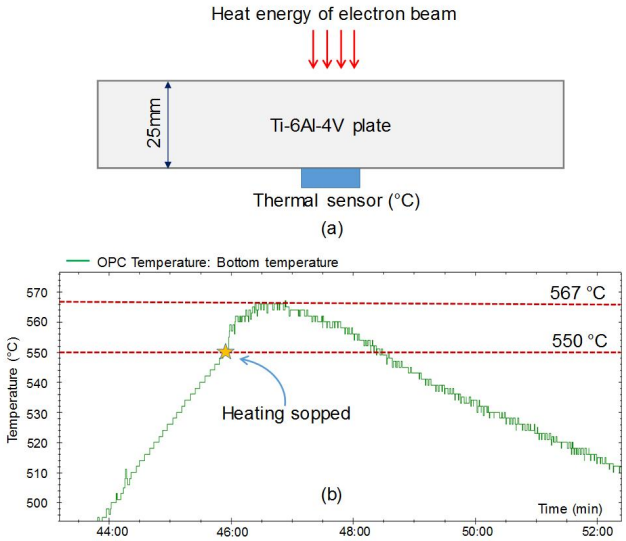

Fig. 3 Experiment to determine temperature of the top surface in preheating: (a) titanium plate with the thermal sensor was placed on the build table of the machine; (b) the temperature graph obtained by the thermal sensor

Moreover, before the deposit of the first powder layer, an electron beam scanning in the melting mode was done in order to configure the top of titanium plate in a configuration closed to the one of a "standard" melted powder layer. Thus, the build feature process was conducted through two steps (Fig. 4). First, the Ti-6Al-4V plate was heated by electron beam until the thermal sensor shows a value of 720^{o}C (namely, the top surface of plate was being heated at about 740^{o}C). Then, the powder layer deposition on the plate was conducted as in normal EBM process until the features are fully built. The built features were presented in Fig. 2.

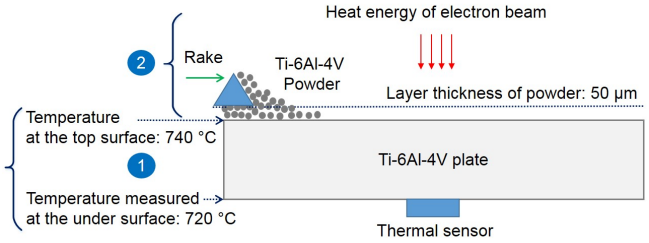

Fig. 4 Building feature process: (1) preheating titanium plate, and (2) building feature

2.4 Metallography and Hardness testing

A sample was cut from EBM-built feature and titanium plate by a wire Electrical Discharge Machining (EDM) machine. This allows an effortless cutting and a limited heating the sample material. Then, the surface affected by EDM cutting was polished and chemically etched (Fig. 5a). This assured that the analyzed material was well extracted from EBM-built feature and titanium plate. The microstructures of the sample were observed by using an Olympus BX51M optical microscope.

A Matsuzawa microhardness tester was also used to determine the Vickers microhardness of the sample. The microstructures and microhardness were examined in three zones: the EBM-built zone, the heat affected zone (HAZ) and the titanium plate zone, as shown in Fig. 5b.

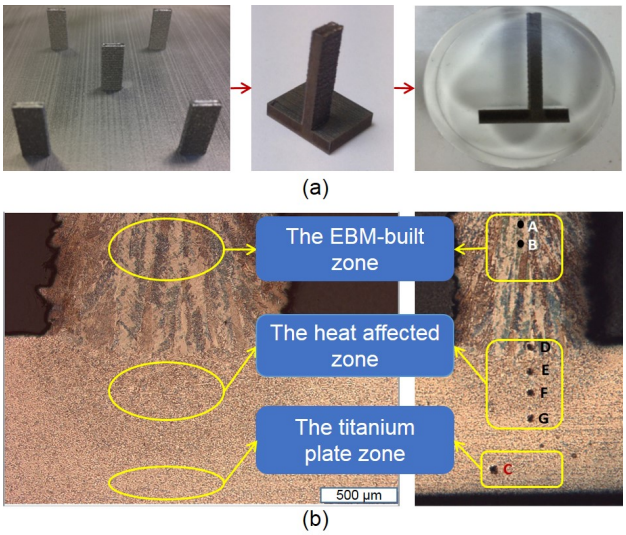

Fig. 5 Sample for microstructure and microhardness investigation: (a) Operations of cutting, polishing and chemically etching the sample; and (b) three zones for observing the microstructures and measuring hardness

2.5 Tensile testing

The tensile testing was performed at room temperature. The sample was fixed on the tensile test machine using a specific attachment system at the bottom (Fig. 6a-b). The upper part of the sample used standard fixtures of the tensile testing machine (DY 35, 20 KN) (Fig. 6c). The tensile testing was conducted in the vertical orientation with a crosshead speed of 1 μm/s. When the force of traction reached 6048 N, the sample broke in the interface zone between the EBM-built feature and the titanium plate (Fig. 6d).

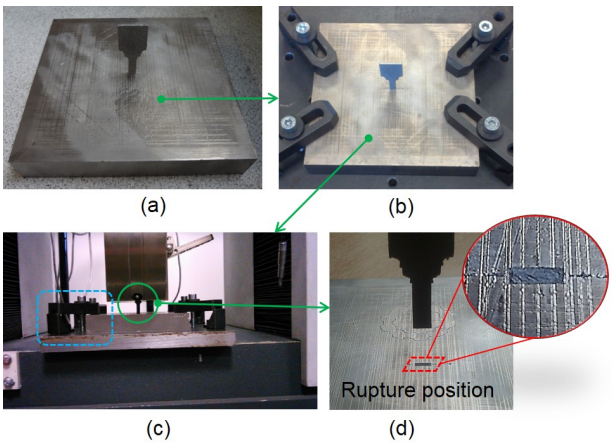

Fig. 6 Installation of the sample on the machine and the tensile testing: (a) tensile test sample; (b) Clamping the test sample on the support by the adjustable straps; (c) Installation the sample and the support on the machine; and (d) broken sample

3 Results and Discussion

3.1 Microstructure

3.1.1 Microstructures of initial Ti-6Al-4V plate and titanium plate zone

Fig. 7a shows the microstructures of the initial Ti-6Al-4V plate. It is a bimodal (or duplex) microstructure composed of α lamellae embedded in a β matrix and surrounded by equiaxed α grains. This microstructure is typical for a titanium alloy deformed below β transus and recrystallized. The microstructures of the titanium plate zone after EBM process (Fig. 7b) are similar to those of the initial Ti-6Al-4V plate. It is clear that there was no microstructural change in this zone. This is because its temperature was maintained at 700 - 740^{o}C below the β transus temperature of 994^{o}C [39]. The microstructure of the titanium plate after fabrication is still bimodal but exhibits a larger number of lamellae (Fig. 7b) than those of the initial titanium plate (Fig. 7a). This may be due to the heating of the plate during the EBM process.

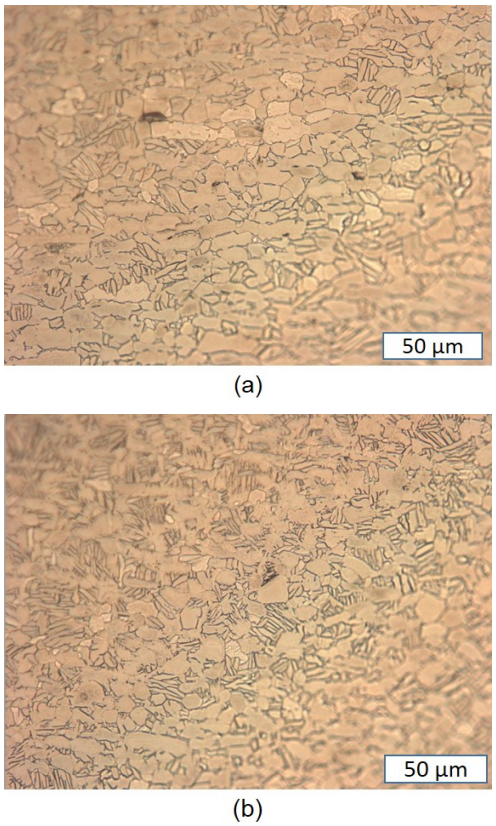

Fig. 7 Microstructures of initial Ti-6Al-4V plate (a), and the titanium plate zone after fabrication (b): duplex microstructure (α lamellae embedded in a β matrix and surrounded by equiaxed α grains)

3.1.2 EBM-built zone microstructures

The micrographs of the EBM-built zone (Fig. 8) show a very fine microstructure when compared to those of initial Ti-6Al-4V plate. Fig. 8a shows the bulk microstructure which is composed of columnar prior β grains growing along the build direction and delineated by grain boundary α. The microstructures inside the columnar prior β grains are typical $\alpha + \beta$ structures with both colony and Widmanstätten morphology of α platelets (Fig. 8b). This microstructure is mainly composed of α phase and a small amount of β; the α phase possess a lamellar morphology with β surrounding the α lamellae boundary. These are comparable with that reported in literature [26, 29]. The major difference in microstructures of the EBM-built zone and the titanium plate zone is due to the high cooling rates of material process in EBM above the β transus. In addition, the build chamber of EBM system is maintained at a temperature of 700 - 740^{o}C during the build process (namely, the material cools down to an isothermal temperature of 700 - 740^{o}C). After completion of the build, the built sample was slowly cooled from 740^{o}C to room temperature within the build chamber that results in the formation of α platelets and prevents the production martensitic α'.

3.1.3 Heat affected zone (HAZ) microstructures

Fig. 9a shows that there is a limit zone between the EBM-built zone and the HAZ. The limit zone also has the lamellar structure of α phase within the columnar prior β grains, especially in the part nearby the EBM-built zone (Fig. 9b). The HAZ presents a microstructure gradient from fully lamellar to duplex. At the top of the HAZ, the microstructure (previously duplex) changed completely to fully lamellar since the temperature was high enough to allow a annealing in the β phase. However, when leaving the top of the HAZ, only a fraction of the microstructure changed to a lamellar microstructure. Where the temperature did not reach the β transus, the microstructure has not changed from the initial duplex microstructure [39, 40].

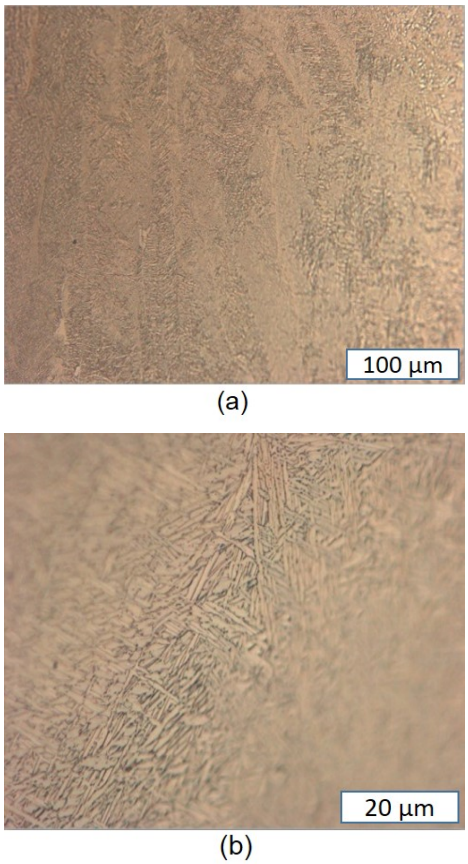

Fig. 8 Microstructures in the EBM-built zone: (a) bulk microstructure (columar prior β grains and delineated by grain boundary α); (b) microstructures inside the columnar prior β grains ($\alpha+\beta$ structures with both colony and Widmanstätten morphology of α platelets)

3.2 Mechanical properties

3.2.1 Microhardness

Table 3 presents the values of Vickers hardness measured in three zones (Fig. 5b). The microhardness of the EBM-built zone, measured at two points A and B, has the highest value, which are comparable to those presented in Table 1. While the microhardness of the HAZ, measured at four points D, E, F and G, is smaller, and decreasing along the depth of HAZ zone with an average value of 362 HV. The microhardness of the titanium plate zone, measured at the point C, is similar to that of initial Ti-6Al-4V plate (362 HV). These results seem coherent with the microstructure observed in Section 3.1 because the Vickers hardness generally decreases when the size and thickness of laminar α/β phase increase.

3.2.2 Tensile properties

Due to the deformation of the bottom fixture system during the tensile testing (Fig. 6c), it was not possible to measure the sample's elongation. In this case, we only know the value of traction force (6048 N) at the time the sample broke. To well explain the results of the tensile testing, it is necessary to examine the normal stresses of the sample, as well as their concentration in the interface zone between the EBM-built feature and the

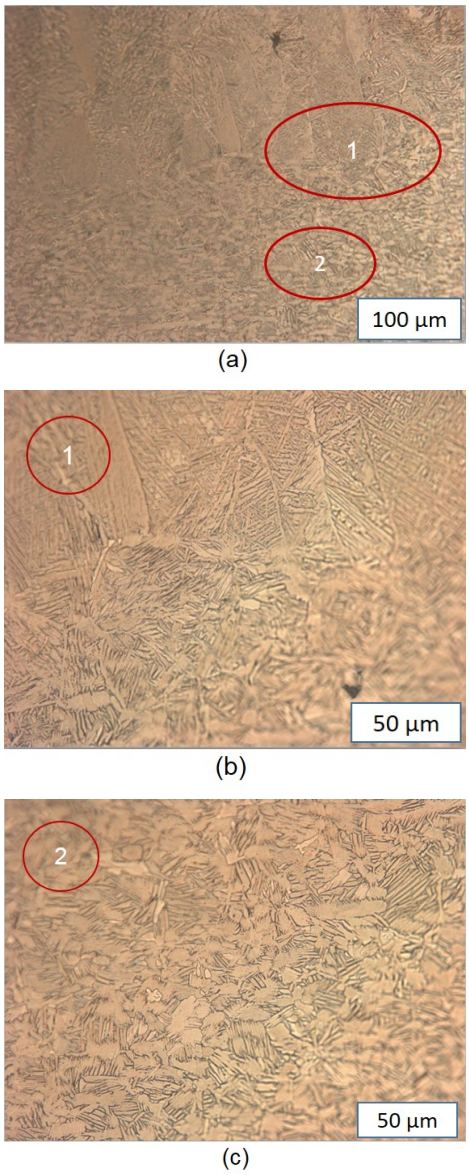

Fig. 9 Microstructure in the HAZ: (a) lower magnification; (b) the lamellar structure of α phase within the columnar prior β grains near the EBM-built zone (the limit zone (1)); and (c) duplex microstructure near titanium plat zone (zone (2))

titanium plate. In this study, a simulation of the tensile testing was conducted. In fact, the total roughness of EBM-built feature surfaces is significantly important (Fig. 10a). Hence, it must be taken into account in the calculation of the dimensions of the model. According to Suard et al. [22], the efficient volume (illustrated by red zone in Fig. 10b) represented more than 80% when the diameter of EBM-built cylinder is larger than 2 mm. In other case study, they showed that the total roughness of surfaces constructed from the Ti-6Al-4V powder by EBM, presents a value of 213 μm. From this value

Table 3 Microhardness (HV) of the test sample

Measure location	Vickers Hardness (HV)
The EBM-built zone	
A	393
B	387
Average value	390
The heat affected zone (HAZ)	
D	385
E	369
F	347
G	348
Average value	362
The titanium plate zone	
C	362

and the measured dimensions of EBM-built feature, the efficient dimensions of EBM-built feature (small cuboid shown in Fig. 11) were approximately calculated.

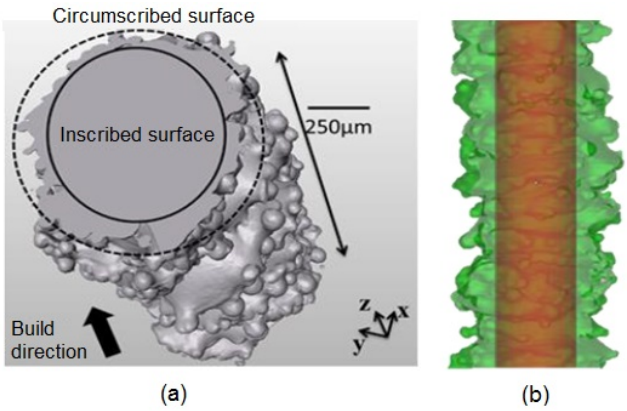

Fig. 10 Appearance and efficient volume of EBM-built cylinder: (a) Tomographic reconstruction of a 1 mm cylinder with the parameters of inscribed and circumscribed surface; (b) reconstruction of the inscribed cylinder (red) inside the real cylinder (green) [22]

During the tensile testing, the bottom of the titanium plate was clamped on the tensile machine. Moreover, the same boundary condition of the actual tensile testing has been used for the simulation. Consequently, to save the time of finite element calculation, the dimensions of plate model were reduced from 150 x 150 x 25 mm to 20 x 20 x 10 mm. In addition, a small joining radius of 80 μm between the EBM-built feature and the plate was also made (see Fig. 11). This value was estimated from the micrograph of the cut sample (Fig. 5b) and the powder size. The model of tensile test simulation is presented in Fig. 11.

The simulation was conducted by using ANSYS software (version 15.0 Academic). A traction force of 6048

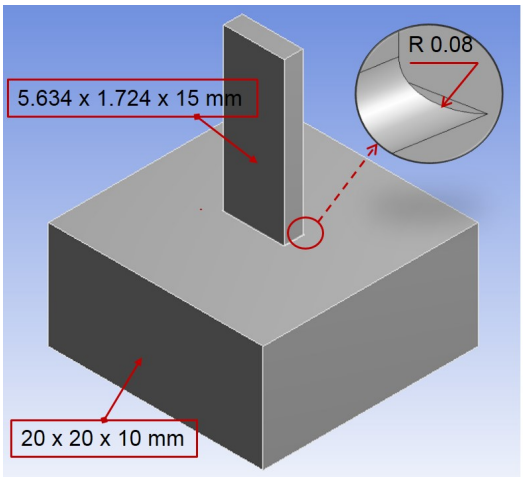

Fig. 11 The model of tensile test simulation

N was put at the top surface of EBM-built feature along the traction direction. The under surface of model was fixed. The titanium alloy, Ti-6Al-4V, which has the modulus of elasticity $E = 114$ GPa and the Poisson's ratio $\nu = 0.34$, was used for the model of simulation. The mesh model and normal stress results of simulation are presented in Fig. 12. It shows that the normal stress in the zone nearby the interface between the small feature and the plate has the highest values (Fig. 12b). This concentration of stresses is due to the shape of sample. The maximum value of normal stress reached 1284.7 MPa. It is higher than the ultimate tensile rupture (1200 MPa) of titanium alloy. Thus, the sample was broken in the interface zone when the traction force reached 6048 N. The simulation considers a perfect bond between the titanium plate and the EBM-built feature. It also suggests a breaking of the sample for a force of 6048 N. Thus, the experimental bonding can be considered to be strong. Moreover, in the Fig. 6d, it clearly showed that there is a small depression on the plate at the rupture position. This means that the EBM-built feature has a strong bond with the plate and behaves as a unique part. More important, this demonstrates that we can build the new feature on the existing part to obtain a new part by EBM technology.

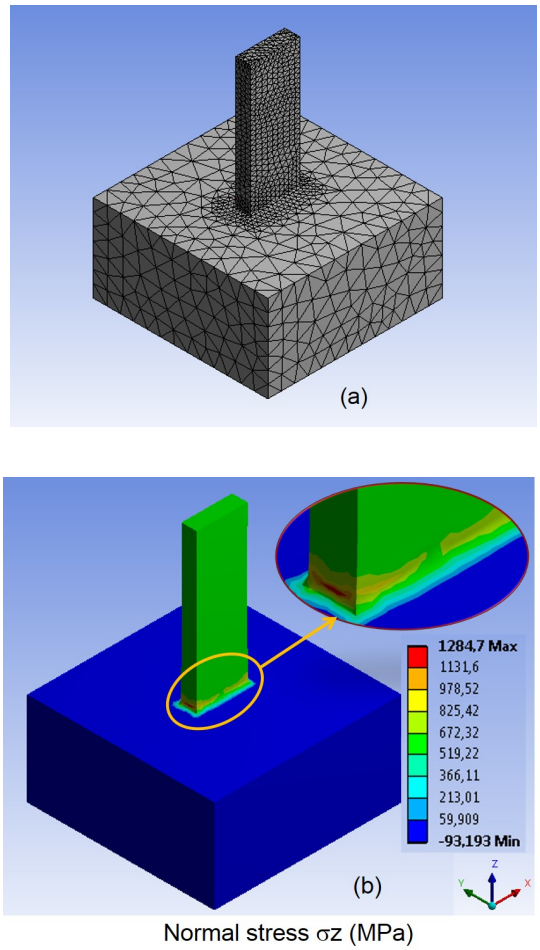

Fig. 12 (a) Meshing model; and (b) normal stress result of simulation

4 Conclusions and future work

This research demonstrated the ability of EBM technology for building new entities from an existing part. In this work, prior studies associated with EBM technology, which mainly focused on the microstructure and mechanical properties of EBM-built parts, or the effects of EBM process parameters on the part quality, were firstly presented. These offer an understanding of EBM process and quality of Ti-6Al-4V EBM-built parts (e.g., microstructure, mechanical properties). Then, an EBM machine was used to build new Ti-6Al-4V features on the Ti-6Al-4V plates considered as existing parts, resulting in new entities/new parts. The samples were then investigated in terms of their microstructures and mechanical properties. The obtained results demonstrated that EBM technology is capable of building new features with good microstructures and mechanical properties, which were comparable to those reported in the literature. The microstructure observation showed that the control of the temperature for melting in EBM process allowed a microstructural gradient from fully lamellar to bi-modal. It is a promising result to achieve a strong bond between new EBM-built features and the titanium plate. Finally, the results of the tensile testing and the tensile test simulation validated this prediction - a strong bond between EBM-built features and existing part was achieved. In addition, the microstructures of the titanium plate zone did not changed, meaning that the EBM process has no significant effect on the microstructure and mechan-

ical properties of the titanium plate (i.e. existing part); thus, the initial properties of existing part were preserved. These results are the first important evidences to develop a new remanufacturing strategy, which is capable of transforming an EoL part/existing part into a new part without returning to the level of raw material (as presented in Ref. [41]).

This research is one of the first studies on the use of AM technologies for remanufacturing, in which we have investigated the build of new features on existing part with the same material (Ti-6Al-4V) by EBM. Future work is also interesting to consider this problem with other materials, as well as with other AM technologies (e.g., SLM, DMD, CLAD). Moreover, other mechanical properties (e.g., fatigue, shear strength) of the built samples are also necessary elements that have to be investigated.

Acknowledgements The authors would like to thank Rhône-Alpes Region of France for its support in this project.

References

1. Guo N, Leu M (2013) Additive manufacturing: technology, applications and research needs. Front Mech Eng 8(3):215-243. doi:10.1007/s11465-013-0248-8
2. Frazier WE (2014). Metal Additive Manufacturing: A Review. J Mater Eng Perform 23(6):19171928. doi:10.1007/s11665-014-0958-z
3. Huang S, Liu P, Mokasdar A, Hou L (2013) Additive manufacturing and its societal impact: a literature review. Int J Adv Manuf Technol 67(5-8):1191-1203. doi:10.1007/s00170-012-4558-5
4. Gibson I, Rosen DW, Stucker B (2010) Additive Manufacturing Technologies. Boston, MA: Springer US. doi:10.1007/978-1-4419-1120-9
5. ASTM F2792-10e1 Standard Terminology for Additive Manufacturing Technologies, ASTM International, West Conshohocken, PA, 2010. http://www.astm.org
6. Atzeni E, Salmi A (2012) Economics of additive manufacturing for end-usable metal parts. Int J Adv Manuf Technol 62:1147-1155. doi:10.1007/s00170-011-3878-1
7. Tang Y, Kurtz A, Zhao Y (2015) Bidirectional Evolutionary Structural Optimization (BESO) based design method for lattice structure to be fabricated by additive manufacturing. Comput-Aided Des 69:91101. doi:10.1016/j.cad.2015.06.001
8. Klahn C, Leutenecker B, Meboldt M (2014). Design for Additive Manufacturing - Supporting the Substitution of Components in Series Products. Procedia CIRP 21:138143. doi:10.1016/j.procir.2014.03.145
9. Gong X, Anderson T, Chou K (2014) Review on powder-based electron beam additive manufacturing technology. Manuf Rev 1(2). doi:10.1051/mfreview/2014001
10. Huang R, Riddle M, Graziano D, Warren J, Das S, Nimbalkar S, Cresko J, Masanet E (2015) Energy and emissions saving potential of additive manufacturing: the case of lightweight aircraft components. J Clean Prod. doi:10.1016/j.jclepro.2015.04.109
11. Gebler M, Schoot Uiterkamp AJM, Visser C (2014) A global sustainability perspective on 3D printing technologies. Energy Policy 74:158167. doi:10.1016/j.enpol.2014.08.033
12. Cheng B, Chou K (2015) Geometric consideration of support structures in part overhang fabrications by electron beam additive manufacturing. Comput-Aided Des 69:102111. doi:10.1016/j.cad.2015.06.007
13. Vayre B, Vignat F, Villeneuve F (2013) Identification on Some Design Key Parameters for Additive Manufacturing: Application on Electron Beam Melting. Procedia CIRP 7:264-269. doi:10.1016/j.procir.2013.05.045
14. Arcam AB Corporation. Available at: http://www.arcam.com/
15. Murr LE, Gaytan SM, Ceylan A, et al (2010) Characterization of titanium aluminide alloy components fabricated by additive manufacturing using electron beam melting. Acta Mater 58(5):1887-1894. doi:10.1016/j.actamat.2009.11.032
16. Cormier D, Harrysson O, West H (2003) Characterization of high alloy steel produced via electron beam melting. Proc Solid Free Fabr Symp:548-558
17. Murr LE, Martinez E, Gaytan SM, et al (2011) Microstructural Architecture, Microstructures, and Mechanical Properties for a Nickel-Base Superalloy Fabricated by Electron Beam Melting. Metall Mater Trans A 42(11):3491-3508. doi:10.1007/s11661-011-0748-2
18. Murr LE, Martinez E, Pan XM, et al (2013) Microstructures of Rene 142 nickel-based superalloy fabricated by electron beam melting. Acta Mater 61(11):4289-4296. doi:10.1016/j.actamat.2013.04.002
19. Ramirez DA, Murr LE, Martinez E, et al (2011) Novel precipitate-microstructural architecture developed in the fabrication of solid copper components by additive manufacturing using electron beam melting. Acta Mater 59(10):4088-4099. doi:http://dx.doi.org/10.1016/j.actamat.2011.03.033
20. Frigola P, Harrysson OA, Ramirez DA (2014) Fabricating Copper Components with Electron Beam Melting. Adv Mater Process 172(7) (ASM Interna-

tional)
21. Koike M, Martinez K, Guo L, Chahine G, Kovacevic R, Okabe T (2011) Evaluation of titanium alloy fabricated using electron beam melting system for dental applications. J Mater Process Technol 211(8):1400-1408. doi:10.1016/j.jmatprotec.2011.03.013
22. Suard M, Lhuissier P, Dendievel R, Blandin J-J, Vignat F, Villeneuve F (2014) Towards stiffness prediction of cellular structures made by electron beam melting (EBM). Powder Metall 57(3):190-195. doi:10.1179/1743290114Y.0000000093
23. Lütjering G, Williams JC (2007) Titanium, 2nd ed. Springer, Berlin
24. Karlsson J, Snis A, Engqvist H, Lausmaa J (2013) Characterization and comparison of materials produced by Electron Beam Melting (EBM) of two different Ti6Al4V powder fractions. J Mater Process Technol 213(12):2109-2118. doi:10.1016/j.jmatprotec.2013.06.010
25. Koike M, Greer P, Owen K, et al (2011) Evaluation of Titanium Alloys Fabricated Using Rapid Prototyping Technologies-Electron Beam Melting and Laser Beam Melting. Materials (Basel) 4(12):1776-1792. doi:10.3390/ma4101776
26. Rafi HK, Karthik NV, Gong H, Starr TL, Stucker BE (2013) Microstructures and Mechanical Properties of Ti6Al4V Parts Fabricated by Selective Laser Melting and Electron Beam Melting. J Mater Eng Perform 22(12):3872-3883. doi:10.1007/s11665-013-0658-0
27. Facchini L, Magalini E, Robotti P, Molinari A (2009) Microstructure and mechanical properties of Ti-6Al-4V produced by electron beam melting of pre-alloyed powders. Rapid Prototyp J 15(3):171-178. doi:10.1108/13552540910960262
28. Murr LE, Quinones SA, Gaytan SM, et al (2009) Microstructure and mechanical behavior of Ti-6Al-4V produced by rapid-layer manufacturing, for biomedical applications. J Mech Behav Biomed Mater 2(1):20-32. doi:10.1016/j.jmbbm.2008.05.004
29. Al-Bermani SS, Blackmore ML, Zhang W, Todd I (2010) The Origin of Microstructural Diversity, Texture, and Mechanical Properties in Electron Beam Melted Ti-6Al-4V. Metall Mater Trans A 41(13):3422-3434. doi:10.1007/s11661-010-0397-x
30. Syam WP, Al-Shehri HA, Al-Ahmari AM, Al-Wazzan KA, Mannan MA (2012) Preliminary fabrication of thin-wall structure of Ti6Al4V for dental restoration by electron beam melting. Rapid Prototyp J 18(3):230-240. doi:10.1108/13552541211218180
31. Guo C, Ge W, Lin F (2015) Effects of scanning parameters on material deposition during Electron Beam Selective Melting of Ti-6Al-4V powder. J Mater Process Technol 217:148-157. doi:10.1016/j.jmatprotec.2014.11.010
32. Weiwei H, Wenpeng J, Haiyan L, Huiping T, Xinting K, Yu H (2011) Research on Preheating of Titanium Alloy Powder in Electron Beam Melting Technology. Rare Met Mater Eng 40(12):2072-2075. doi:10.1016/S1875-5372(12)60014-9
33. Morrow WR, Qi H, Kim I, Mazumder J, Skerlos SJ (2007) Environmental aspects of laser-based and conventional tool and die manufacturing. J Clean Prod 15(10):932-943. doi:10.1016/j.jclepro.2005.11.030
34. Jhavar S, Paul CP, Jain NK (2013) Causes of failure and repairing options for dies and molds: A review. Eng Fail Anal 34:519-535. doi:10.1016/j.engfailanal.2013.09.006
35. Wilson JM, Piya C, Shin YC, Zhao F, Ramani K (2014) Remanufacturing of turbine blades by laser direct deposition with its energy and environmental impact analysis. J Clean Prod 80:170-178. doi:http://dx.doi.org/10.1016/j.jclepro.2014.05.084
36. Nan L, Liu W, Zhang K (2010) Laser remanufacturing based on the integration of reverse engineering and laser cladding. Int J Comput Appl Technol 40(4):254-262. doi:10.1504/IJCAT.2010.032200
37. Dutta B, Froes FH (2014) Additive manufacturing of titanium alloys. Adv Mater Process 172:18-23
38. Terrazas CA, Gaytan SM, Rodriguez E, et al (2014) Multi-material metallic structure fabrication using electron beam melting. Int J Adv Manuf Technol 71(1-4):33-45. doi:10.1007/s00170-013-5449-0
39. Cottam R, Brandt M (2011) Laser Cladding of Ti-6Al-4V Powder on Ti-6Al-4V Substrate: Effect of Laser Cladding Parameters on Microstructure. Phys Procedia 12:323-329. doi:10.1016/j.phpro.2011.03.041
40. Safdar A (2012) A Study on Electron Beam Melted Adnan Safdar. Ph.D. Thesis, Lund University, Lund, Sweden
41. Le VT, Paris H, Mandil G (2015) Using additive and subtractive manufacturing technologies in a new remanufacturing strategy to produce new parts from End-of-Life parts. 22nd French Congr Mech (CFM2015), Lyon, France, 24-28 Aug 2015